Check for updates

Comparison of Li, Na, Mg and Al-ion insertion in vanadium pentoxides and vanadium dioxides†

Vadym V. Kulish [ID] and Sergei Manzhos [ID]*

Vanadium oxides (VO) are among the most promising electrode materials for advanced electrochemical batteries since they are able to operate in most major types of batteries (Li, Na, Mg and Al-ion). The practical development of VO electrodes, however, is complicated by the presence of multiple VO stoichiometries and phases with distinctly different lattice stabilities, electronic properties and, hence, metal ion insertion thermodynamics and kinetics. We present a systematic comparative *ab initio* study of four most stable VO phases (α-V_2O_5, β-V_2O_5, VO_2(R) and VO_2(B)) and their interaction mechanism with Li, Na, Mg, and Al atoms. Our results show that among the studied phases, rutile VO_2(R) exhibits the largest Al binding energy and a low Al diffusion barrier, which makes it quite promising for Al-ion batteries. At the same time, the β-V_2O_5 phase exhibits the highest binding energy for Mg insertion and significant reduction of the Mg diffusion barrier compared to conventionally used α-V_2O_5. Our results highlight the benefits of rational phase engineering and may assist further experimental studies of high performance VO electrodes for Na, Mg, and Al-ion batteries.

1. Introduction

Affordable energy storage is essential for the practical realization of hybrid or all-electric vehicles and grid integration of renewable sources (*e.g.* solar and wind). Although Li-ion batteries provide the highest energy density among commercial battery technologies, the limited and inhomogeneous global distribution of Li resources may hinder their long-term and large-scale applications. Among the alternative technologies, Na, Mg and Al-ion batteries are attracting an ever-growing research attention due to their advantages in elemental abundance and environment-friendly chemistry. Moreover, Mg-ion and Al-ion batteries can operate with metallic Mg and Al anodes, offering the benefits of low cost, dendrite-free deposition during charging and high volumetric capacity. However, the identification of suitable cathode materials has been a major challenge in the development of Na, Mg and Al-ion batteries. Due to the larger ion size or multivalency, the storage of Na, Mg, and Al is associated with low binding energies to an electrode material (compared with the metal's cohesive energy) and high energy barriers for ionic diffusion.[1–6] Thus, identification of suitable cathode materials specific for post-lithium batteries is necessary and requires thorough understanding of the basic insertion mechanisms.

Department of Mechanical Engineering, National University of Singapore, Block EA #07-08, 9 Engineering Drive 1, Singapore 117576, Singapore. E-mail: mpemanzh@nus.edu.sg

Vanadium oxides (VO) are among the few materials that are able to operate as electrodes for the most types of batteries.[7–14] For example, layered V_2O_5 has shown Mg storage capacities of >150 mA h g^{-1} at 2.3–2.6 V *vs.* Mg/Mg^{2+}.[15] Al insertion in V_2O_5 has been demonstrated as well, although at a rather low voltage of about 1 V (*vs.* Al/Al^{3+}).[16,17] VO_2 exhibits high Li storage capacity (320 mA h g^{-1}) and good stability resulting from edge-sharing VO_6 octahedra bilayers.[18,19] Despite these promising studies, a systematic understanding of VO electrodes is currently lacking, mainly due to the presence of multiple stoichiometries and phases, such as α-V_2O_5, β-V_2O_5, VO_2(R), VO_2(B), V_6O_{13}, V_3O_7, *etc.*[20,21] The crystalline and electronic structures of VO polymorphs are complex with distinctly different lattice symmetries, electronic properties and, hence, different metal-ion insertion thermodynamics and kinetics. It would be highly desirable to rationally select the best VO phase for a given type of battery. So far, the layered V_2O_5 has been the most studied VO phase and may serve as a convenient benchmark system.[22–28] Carrasco *et al.* employed van der Waals (vdW)-inclusive methods with nonlocal density functionals to investigate the Li and Na insertion into α-V_2O_5.[29,30] However, vdW-corrected methods may overestimate the voltages and diffusion barriers in electrode materials.[4,31] Gautam *et al.*[32–35] and Zhou *et al.*[36] theoretically investigated Mg insertion in orthorhombic V_2O_5 using DFT+U methods.

While recent studies investigated vanadium pentoxides as cathode materials, there have been no reports on Li, Na, Mg and Al insertion in VO_2 compounds. Moreover, there have been no theoretical study comparing with the same computational setup the insertion energetics into multiple VO compounds, such as

α-V$_2$O$_5$, β-V$_2$O$_5$, VO$_2$(R), and VO$_2$(B). In this paper, we attempt to fill this knowledge gap, and more importantly, we investigate the potential of VO$_2$ phases as a potential cathode materials for Li, Na, Mg, and Al-ion batteries. Our theoretical work fits very well with the latest experimental advances in controlled growth and epitaxial stabilization of the VO polymorphs as reported recently.[11,37] Theoretical insights from our work would help the development of high-performance VO electrodes for Li, Na, Mg, and Al-ion batteries.

2.   Computational methods

Calculations were performed within the density functional theory (DFT) framework, as implemented in the VASP 5.3 package.[38] The core electrons were treated within the projector augmented wave (PAW) method.[39,40] Exchange-correlation effects were described with the generalized gradient approximation and the PBEsol functional.[41] For comparison, we have also used PBE functional[42] and van der Waals-corrected D2 method of Grimme.[43] The following valence electron configurations were used: Li (2s^1), Na (3s^1), Mg (2p^6 3s^2), Al (3s^2 3p^1), V (3p^6 3d^4 4s^1) and O (2s^2 2p^4). The total energies of the VO supercells were calculated using converged Γ-centered Monkhorst–Pack k-point grids.[44] The plane-wave cutoff was 500 eV. The Gaussian smearing with a smearing factor of 0.1 eV was used in all calculations. The optimized structures were obtained by relaxing all atomic positions and lattice parameters using the conjugated gradient algorithm until all forces are smaller than 0.01 eV Å^{-1}. With the selected modeling parameters, the predicted lattice constants of the VO phases agree well with the experimental data (Table 1). The amount of charge transfer between the metal ion atom and VO host is estimated from the grid-based Bader charge analysis.[45] Large supercells of VO were used, describing insertion at the dilute concentration (1–1.5 at%). In such a way, metal–metal interactions can be neglected and the interaction of the isolated inserted atom with VO can be studied. We used a ($3 \times 1 \times 3$) supercell for α-V$_2$O$_5$ (127 atoms), a ($3 \times 1 \times 1$) supercell for β-V$_2$O$_5$ (85 atoms), a ($2 \times 2 \times 4$)

supercell for VO$_2$(R) (97 atoms), and a ($1 \times 3 \times 2$) supercell for VO$_2$(B) (145 atoms). Activation barriers for diffusion are calculated using the climbing-image nudged elastic band (CI-NEB) method.[46] The CI-NEB calculations were performed using 3–6 images, and the initial guess of the migration pathway has been generated by linear interpolation between the initial and final points of the diffusion path. The geometry and energy of the images were then relaxed until the largest norm of the force orthogonal to the path was smaller than 0.02 eV Å^{-1}. To account for the on-site Coulomb interactions between the V 3d electrons, we performed DFT+U calculations by adding an effective parameter, U_{eff}, as introduced by Dudarev *et al.*[47] As suggested by Ceder *et al.*,[48] we have used $U_{eff} = 3.0$ eV for vanadium. Spin polarization is included, and all calculations were performed for the ferromagnetic (FM) spin ordering. In fact, it is reported in the literature that lithiated phases with FM ordering are lower in energy than those with AFM ordering.[49]

The insertion (binding) energy (E_b) per inserted atom is estimated as

$$E_{ins} = \frac{E_{M-VO} - E_{VO} - nE_M}{n} \quad (1)$$

where E_{M-VO} is the total energy of the VO crystal with n inserted M (M = Li, Na, Mg or Al) atoms, E_{VO} is the total energy of pristine VO, and E_M is the energy per atom of M in its bulk phase (bcc Li and Na, hcp Mg and fcc Al). A negative value of E_b indicates that the metal insertion is thermodynamic favorable. We note that the binding energy can be used to estimate the average voltage of the electrode for insertion up to the concentration or specific capacity corresponding to n:

$$V = -\frac{E_{ins}}{ez} \quad (2)$$

where e is the elementary charge and z is the number of electrons transferred per inserted atom ($z = 1$ for Li and Na, 2 for Mg, and 3 for Al).[50]

3.   Results and discussion

3.1.   Crystal structures of pure VO phases

We consider two polymorphs of vanadium pentoxide (V$_2$O$_5$): α-V$_2$O$_5$ and β-V$_2$O$_5$ (Fig. 1a and b). From the experimental studies, α-V$_2$O$_5$ is the most stable bulk phase at temperatures below 400 °C.[51] The α-V$_2$O$_5$ has a layered crystal structure (space group *Pmmn*, no. 59), consisting of layers of alternating corner- and edge-sharing VO$_5$ pyramids. Each V atom is five-coordinated with four V–O bonds of 1.78–1.86 Å and one short double V=O bond of 1.58 Å, which forms the apex of the VO$_5$ pyramid. The key difference between α-V$_2$O$_5$ and β-V$_2$O$_5$ phases is the layer stacking order. In metastable β-V$_2$O$_5$ (space group *Cmcm*, no. 63), alternate layers are displaced by $a/2$, leading to considerable changes in the interlayer spacing (which is larger by >0.5 Å). The adjacent layers are interacting by weak van der Waals (vdW) forces along $c(z)$ direction.

The most stable phase of vanadium dioxide (VO$_2$) is rutile (VO$_2$(R), Fig. 1c), which belongs to the space group $P4_2/mnm$ (136). VO$_2$(R) is stable in the temperature range from 68 °C to

Table 1 Calculated lattice parameters of V$_2$O$_5$ and VO$_2$ phases. The theoretical values are compared to the experimental data

Compound	Functional	a (Å)	b (Å)	c (Å)
α-V$_2$O$_5$	PBE	3.57	11.60	4.54
	PBEsol	3.54	11.55	4.32
	D2-vdW	3.54	11.64	4.40
	Exp[51]	3.56	11.51	4.36
β-V$_2$O$_5$	PBE	11.54	3.56	10.74
	PBEsol	11.50	3.53	10.69
	D2-vdW	11.58	3.52	10.04
VO$_2$(R)	PBE	4.59	4.59	2.85
	PBEsol	4.55	4.55	2.85
	D2-vdW	4.55	4.55	2.84
	Exp[52]	4.55	4.55	2.86
VO$_2$(B)	PBE	12.01	3.73	6.42
	PBEsol	12.02	3.71	6.39
	D2-vdW	12.00	3.70	6.40
	Exp[52]	12.03	3.69	6.42
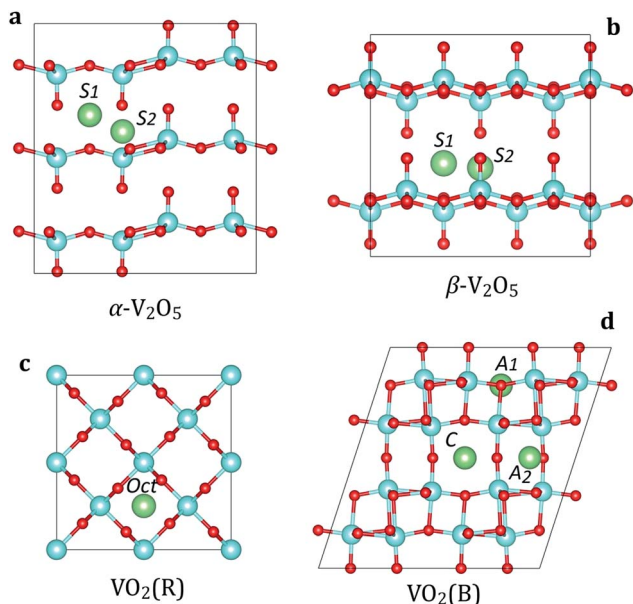
Fig. 1 Crystal structures and insertion sites in the most stable V_2O_5 and VO_2 phases: (a) α-V_2O_5, (b) β-V_2O_5, (c) $VO_2(R)$, and (d) $VO_2(B)$. The V, O and M (M = Li, Na, Mg, Al) atoms are shown in cyan, red and green colors, respectively.

1540 °C.[52] It consists of VO_6 octahedra which share edges, forming tunnel-like structure along the c axis. Our calculated lattice parameters for $VO_2(R)$ are $a = b = 4.55$ Å and $c = 2.85$ Å, close to the experimental values.[52] Each V atom is six-coordinated with two V–O bonds of 1.93 Å and four V–O bonds of 1.92 Å.

The monoclinic polymorph of vanadium dioxide ($VO_2(B)$, Fig. 1d), belonging to the space group $C2/m$ (12), can be synthesized by gentle reduction (hydrothermal treatment) of V_2O_5. $VO_2(B)$ has a larger unit cell as compared to $VO_2(R)$, and can be described as stacking of two identical layers of VO_6 octahedra along b axis. The second layer is shifted with respect to the first one by $\frac{1}{2}$, $\frac{1}{2}$ and 0 along x, y, and z directions, respectively. The VO_6 octahedra are deformed with the V atoms being no longer in their center. Our calculated lattice parameters for $VO_2(B)$ are $a = 12.02$ Å, $b = 3.71$ Å, $c = 6.39$ Å, consistent with experimental data.[52] The calculated V–O bond lengths are 1.87–2.07 Å. In $VO_2(B)$, all VO_6 octahedra are aligned along the same crystallographic orientation.

The calculated structural parameters for VO phases are summarized in Table 1. We can notice that lattice parameters in strongly-bonded $VO_2(R)$ and $VO_2(B)$ phases are reproduced with a good accuracy by all functionals. However, PBE calculations overestimate the interlayer spacing of 4.54 Å in α-V_2O_5 phase. In contrast, PBEsol calculations show an optimal interlayer spacing of 4.32 Å, in good agreement with the experimental value of 4.36 Å. The effect of van der Waals interactions in α-V_2O_5 can also be treated by using the semi-empirical correction scheme of Grimme (DFT-D2).[43] However, studies show that use of vdW-corrected functionals may potentially lead to over-estimated voltages in covalently-bonded phases, such as VO_2.[4]

Therefore, in order to preserve the consistency in the computational setup among both weak and strongly-bonded VO phases, we use the PBEsol functional in all following calculations.

3.2. Energetics of Li, Na, Mg and Al insertion

We first examine the insertion of M atoms (M = Li, Na, Mg and Al) into α-V_2O_5 at the dilute concentration. There are two possible insertion sites for M ions as shown in Fig. 1a. At the S1 site, the M atom is located at the high-symmetry position with equal distances to four vanadyl oxygens (O1) and two bridging oxygens (O2). At the S2 site, the M atoms are located on the line between vanadyl O1 and V atoms. The M atoms at the S1 and S2 sites are six- and four-coordinated, respectively. We find that the inserted M ions strongly prefer to occupy the S1 site. The lattice distortions caused by M insertion are very small, suggesting good stability of V_2O_5 host during battery cycling. When M atom is placed at the S1 site, the four vanadyl O1 atoms move towards the M ion with slight increase in the V–O bond lengths. The results for M insertion at the most stable site (S1) are summarized in Table 2. Importantly, we find that all M atoms (Li, Na, Mg and Al) have negative binding energies in α-V_2O_5. This implies that metal insertion in V_2O_5 is energetically favorable. The insertion voltage at the low concentration follows the trend Li/Na > Mg > Al.

The insertion sites in β-V_2O_5 resemble very closely those in α-V_2O_5 with the same local coordination of M atoms (Fig. 1b). However, we find that M insertion is more energetically favorable in β-V_2O_5 than in the α phase. Although the difference for the Li is quite small, for Na, Mg and Al atoms it is substantial (Table 2). This is directly related to an extra space available

Table 2 Calculated insertion energy (E_{ins}), equiv. voltage for single atom insertion (V), bond length (d_{M-O}), and charge transfer (Q) for the M = Li, Na, Mg, and Al insertion into α-V_2O_5, β-V_2O_5, $VO_2(R)$ and $VO_2(B)$ phases for the minimum-energy insertion sites. The M–O bond lengths in Li_2O, Na_2O, MgO and Al_2O_3 are given for comparison

Compound	Property	Li	Na	Mg	Al
α-V_2O_5	E_{ins} (eV)	−3.13	−3.17	−5.50	−5.11
	V (V)	3.13	3.17	2.75	1.70
	d_{M-O} (Å)	2.20	2.41	2.19	2.10
	Q (|e|)	0.86	0.88	1.60	2.43
	Site	S1	S1	S1	S1
β-V_2O_5	E_{ins} (eV)	−3.35	−3.50	−6.21	−5.32
	V (V)	3.35	3.50	3.10	1.77
	d_{M-O} (Å)	2.31	2.55	2.32	2.12
	Q (|e|)	0.90	0.89	1.65	2.49
	Site	S1	S1	S1	S1
$VO_2(R)$	E_{ins} (eV)	−3.65	−1.09	−3.96	−5.97
	V (V)	3.65	1.09	1.98	1.99
	d_{M-O} (Å)	1.85	1.96	1.87	1.78
	Q (|e|)	0.92	0.87	1.61	2.45
	Site	Oct	Oct	Oct	Oct
$VO_2(B)$	E_{ins} (eV)	−3.11	−2.99	−5.46	−5.76
	V (V)	3.11	2.99	2.73	1.92
	d_{M-O} (Å)	2.01	2.53	2.15	1.75
	Q (|e|)	0.92	0.90	1.61	2.44
	Site	C	C	A1	A1
M-oxide	d_{M-O} (Å)	2.01	2.42	2.12	1.87

for M insertion (the interlayer spacing in β-V_2O_5 is >0.5 Å larger than in α-V_2O_5). We also find that the volume changes in β-V_2O_5 upon M insertion are smaller than in α-V_2O_5, as measured by the change in interlayer spacing. This is beneficial for the long-term cycling of batteries.

In contrast to V_2O_5, the VO_2 polymorphs are considerably less studied as electrode materials. To the best of our knowledge, there have been only limited theoretical studies on the insertion of Li, Na, Mg or Al atoms in VO_2.[53] First, we address the rutile VO_2 phase. There are two possible insertion positions for metal ions in the $VO_2(R)$ structure (Fig. 1c): octahedral (Oct) and tetrahedral (Td). Our calculations show a strong preference for insertion at the Oct site for all atoms. The Td site is energetically metastable, and can be possibly occupied at larger metal ion concentrations. In the following, we discuss the local coordination of inserted Li, Na, Mg and Al on the example of Li. When placed in the octahedral site, the Li atom is six-fold coordinated with two Li–O bonds lengths of 1.78 Å and four of 2.05 Å. In the Td position, the Li atom adopts four-fold coordination forming Li–O bonds of 1.78–1.85 Å. The larger binding energies at the Oct site (by >0.20 eV) show that metal atoms prefer sites with a higher coordination number. The preference for the Oct site can also be rationalized by much more space available for metal atom insertion, leading to smaller structural deformations.

Next, we examine metal ion insertion in the $VO_2(B)$, the second most stable VO_2 phase.[52] We have considered three stable intercalation sites (Fig. 1d), which are denoted as A1, A2, and C. The unit cell of $VO_2(B)$ contains four A1 sites, which are 5-fold coordinated to oxygen atoms; four A2 sites, which are also 5-fold coordinated to oxygen; and two C sites, which have a planar 4-fold coordination. Our calculations show that there is a difference in site preference among metal atoms. Namely, Li and Na favor insertion at the C site. When Li is located at the C site, its position is slightly displaced in the b direction from the ideal coordinates. Similar displacement has also been observed in bronze TiO_2.[54] In contrast, Mg and Al atoms prefer the A1 insertion site.

The preference of insertion at the particular site in $VO_2(B)$ can be rationalized by the interplay of two factors. First, a stable insertion configuration should lead to minimum lattice strains induced by the presence of the cation. This can be achieved by insertion at sites within the more open channel region, such as the C site. Secondly, insertion is favored at sites with effective screening of the electrostatic repulsions due to M–M and M–V ion interactions. Such screening can be enhanced by increasing M–V distances and maximizing the degree of oxygen coordination. The position with the highest degree of oxygen coordination in $VO_2(B)$ corresponds to the five-coordinated A1 site. Overall, it seems that the first argument is dominant for Li and Na atoms. Meanwhile, the insertion of multivalent atoms (Mg and Al) with larger polarization is ruled by the second factor.

The calculated binding energies (Table 2) demonstrate several important differences between V_2O_5 and VO_2 phases. First, Li insertion is energetically favorable in all structures with similar estimated voltages (3.13–3.65 V). This is consistent with experimental voltages[55–57] achieved by vanadium oxides in Li-ion and Mg-ion batteries at the dilute concentrations studied here, which correspond to 8.19, 12.28, 10.09, and 6.73 mA h g^{-1} in α-V_2O_5, β-V_2O_5, $VO_2(R)$, and $VO_2(B)$, respectively. However, the binding energies for Na and Mg in $VO_2(R)$ are significantly reduced, as compared to V_2O_5. For instance, Na insertion energy in $VO_2(R)$ is only −1.09 eV. Due to the larger ionic radius of Na, there is not enough space to its accommodation within the $VO_2(R)$ host. The calculated Na–O bond lengths in $VO_2(R)$ are 1.96 Å, much shorter than the equilibrium Na–O bond of 2.42 Å in Na_2O oxide. On the other hand, the presence of open channels in $VO_2(B)$ leads to the favorable Na insertion with a binding energy of −2.99 eV. Remarkably, the estimated voltage for single Al insertion is greatly increased in $VO_2(R)$ and $VO_2(B)$ as compared to V_2O_5: namely, from 1.70 V in α-V_2O5 to 1.99 V in $VO_2(R)$. In fact, the calculated Al–O bond lengths at the Oct site in $VO_2(R)$ (1.78–1.94 Å) are nearly identical to that of 1.87 Å in Al_2O_3 oxide, suggesting favorable Al insertion. Considering that the low Al insertion voltages have been a major bottleneck for the energy density in Al ion batteries, our results demonstrate that $VO_2(R)$ has a good potential as electrode for Al-ion batteries.

3.3. Electronic structure

Vanadium oxides exhibit a variety of distinctly different electronic properties. In particular, we find that V_2O_5 phases are non-magnetic semiconductors, while VO_2 phases are spin-polarized metals as shown in Fig. 2.

Both pristine α-V_2O_5 and β-V_2O_5 show similar electronic structure. Here, the valence band is formed by O 2p bands, while the top of conduction band mainly originates from V 3d states. The DFT+U-calculated DOS of α-V_2O_5 with Li, Na, Mg and Al inserted atoms are shown in Fig. 3. Upon insertion, the valence shells of the metal atoms are fully ionized, they donate their valence electrons to the host bands. Due to the charge transfer, the Fermi level is shifted towards the conduction band. The insertion of Li, Na, Mg and Al gives rise to midgap state between the conduction and valence bands. These midgap states originate from filling of the lowest-energy nonbonding V 3d states as a result of the electron transfer from the inserted atom. The number of such states is equal to the number of valence electrons transferred. Note that in Li- and Na-inserted systems, the spin-polarized V-3d states are located very near the bottom of the conduction band but are separate from it.

In contrast, VO_2 phases have spin-polarized metallic electronic structure with large density of states at the Fermi level. The states near the Fermi level originate mainly from V 3d bands. The p–d hybridization causes additional O 2p contributions in this energy range resulting from the V 3d–O 2p bonding. Our results for rutile VO_2 agree very well with the literature.[52] We find that metal ion insertion does not noticeably affect the electronic structure of the VO_2 host. In such case, the states originating from the metal ions are covered by the metallic nature of the VO_2 host (see Fig. S1 in the ESI†).

We examined the charge redistribution by plotting the spin density difference. Fig. S2† shows it for the case of Mg insertion in α-V_2O_5, with the number of d-like orbitals equal to the
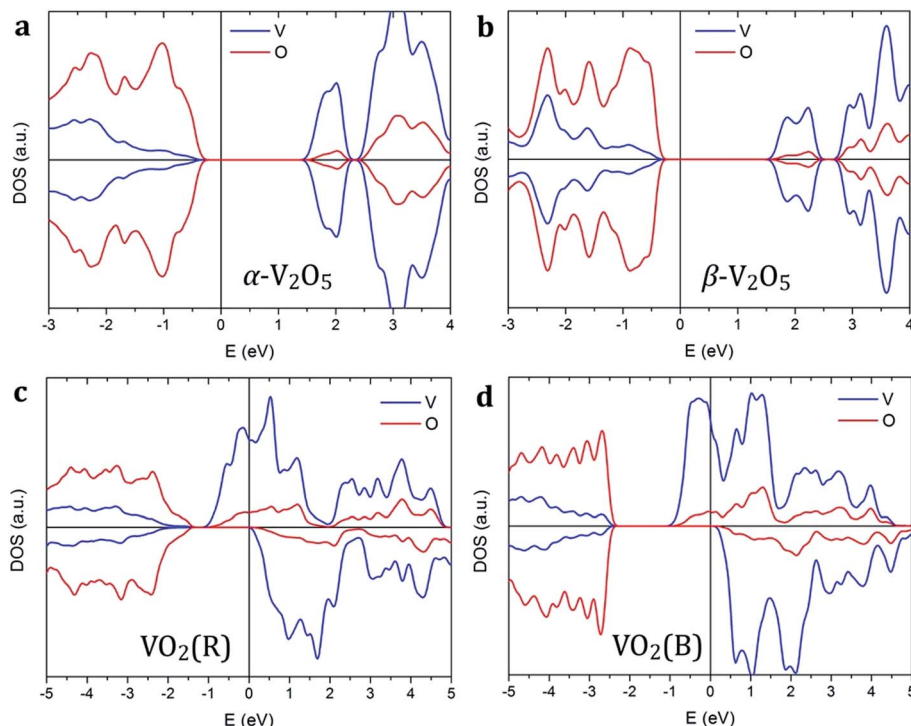
Fig. 2 Spin-polarized density of states of (a) α-V_2O_5, (b) β-V_2O_5, (c) VO_2(R), and (d) VO_2(B). The Fermi level is aligned to zero, indicated by the vertical line.
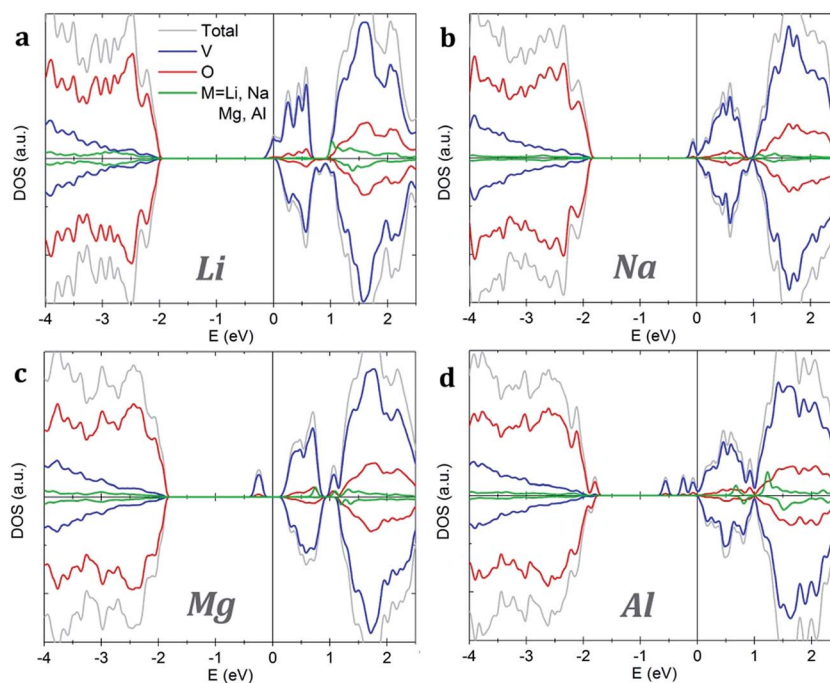

Fig. 3 Density of states of α-V_2O_5 with inserted (a) Li, (b) Na, (c) Mg and (d) Al atoms. The plots are aligned at the Fermi level, indicated by the vertical line.

number of valence electrons donated. For all oxides, we found that the charge accumulation on the V atoms, indicating the reduction of V species. Interestingly, the partial V reduction believed to be from V^{5+} to V^{4+}, as well as the Fermi level shift has

been experimentally observed in X-ray photoelectron spectroscopy (XPS) for Na–V_2O_5.[8] A large fraction of the electron donated by the metal ion to the oxide host is not only transferred to V (thus changing the valence of V according to a conventional
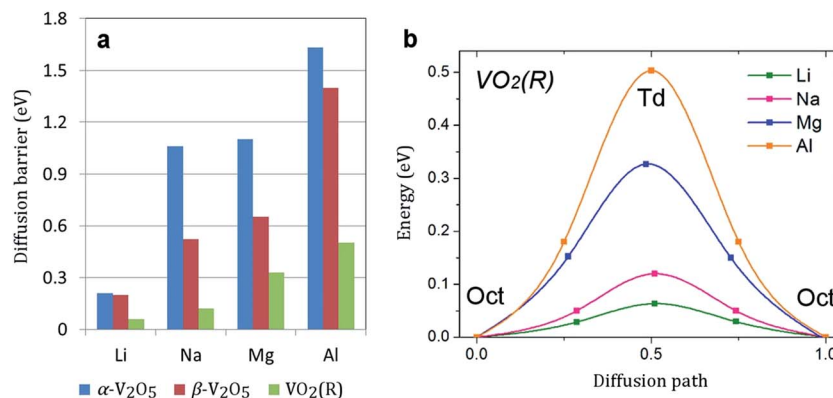
Fig. 4   (a) The calculated diffusion barriers (in eV) in α-V$_2$O$_5$, β-V$_2$O$_5$, and VO$_2$(R). (b) The energy profile for the lowest energy diffusion pathway of Li, Na, Mg, and Al in VO$_2$(R).

chemistry point of view) but is also transferred to oxygen. For example, it was found that about 50% of the charge from Li is transferred to oxygen in VO$_2$. The Bader charge analysis shows that the electron transfer from metal ions to the oxide host is very local. In particular, there is a significant increase in the electron density at the oxygen sites immediately surrounding the inserted metal ions.

3.4.   Diffusion

Facile electron and ionic transport are desirable for fast charge/ discharge rate in electrode materials. Ionic diffusion in α-V$_2$O$_5$ can be presented as a one-dimensional process along the x-axis (the smallest lattice parameter). The calculated diffusion barriers are summarized in Fig. 4a. The energy barrier follows the trend Li < Na < Mg < Al. For all atoms except Li (0.35 eV), the energy barrier is >1 eV, indicating very slow diffusion kinetics. This is consistent with previous works which reported a barrier for Mg diffusion in α-V$_2$O$_5$ of 0.90–1.15 eV.[28,35] The slow Na diffusion is attributed to the large size of Na ions. The slow Mg and Al diffusion can be attributed to the polarization effect of Mg^{2+} and Al^{3+} and strong Mg–O/Al–O interactions. Remarkably, the diffusion barrier can be lowered by a factor of two in β-V$_2$O$_5$ phase (to 0.52 and 0.65 eV for Na and Mg, respectively). Such reduction will lead to much faster charge/discharge rates in Na-ion and Mg-ion batteries.

Metal diffusion in VO$_2$(R) may involve several possible pathways. The pathway with the lowest energy barrier is along the z direction. Most remarkably, we find very low metal ion diffusion barriers in VO$_2$(R). As shown in Fig. 4b, the migration barriers for Mg and Al are only 0.33 and 0.50 eV, respectively. Another possible pathway is located in the xy plane. Here, metal ion diffusion occurs via tetrahedral sites. The energy barrier for this pathway is much higher, which suggests that metal diffusion in VO$_2$(R) is anisotropic. The barrier for Al diffusion is the lowest among all electrode materials for Al-ion batteries reported in the literature. It is comparable to the energy barrier for Li diffusion in high-capacity bulk silicon anode (0.57 eV).[6,58] Considering recent experimental advances in surface-oriented, anisotropic growth of VO$_2$ crystals,[11] we can expect facile diffusion rates in VO$_2$(R) as a potential anode material for Na-ion batteries.

4.   Conclusions

In summary, we presented a comprehensive and truly comparative study of Li, Na, Mg and Al insertion in the most stable VO phases (α-V$_2$O$_5$, β-V$_2$O$_5$, VO$_2$(R) and VO$_2$(B)). We found that the VO$_2$(R) phase exhibits the highest voltage for Al insertion and a low Al diffusion barrier, and may be a potential cathode choice for Al-ion batteries. The β-V$_2$O$_5$ phase may be the most promising VO cathode material for Na-ion and Mg-ion batteries due to much improved diffusion kinetics and sufficiently high voltages. The energy barriers for Na and Mg diffusion in α-V$_2$O$_5$ are rather high (>1 eV). However, we have observed a significant reduction of barriers for Na and Mg diffusion in the β-V$_2$O$_5$ phase (0.52 and 0.65 eV, respectively) leading to potential fast charge/discharge rates. Overall, our study highlights the benefits of rational phase engineering for VO cathode materials in rechargeable batteries.

Acknowledgements

References

1 S. P. Ong, V. L. Chevrier, G. Hautier, A. Jain, C. Moore, S. Kim, X. H. Ma and G. Ceder, $Energy\ Environ.\ Sci.$, 2011, **4**, 3680–3688.
2 V. L. Chevrier and G. Ceder, $J.\ Electrochem.\ Soc.$, 2011, **158**, A1011–A1014.
3 O. Malyi, V. V. Kulish, T. L. Tan and S. Manzhos, $Nano\ Energy$, 2013, **2**, 1149–1157.
4 M. A. Sk and S. Manzhos, $J.\ Power\ Sources$, 2016, **324**, 572–581.
5 F. Legrain, O. Malyi and S. Manzhos, $J.\ Power\ Sources$, 2015, **278**, 197–202.

6 V. V. Kulish, O. I. Malyi, M.-F. Ng, Z. Chen, S. Manzhos and P. Wu, *Phys. Chem. Chem. Phys.*, 2014, **16**, 4260–4267.

7 D. Kundu, B. D. Adams, V. Duffort, S. H. Vajargah and L. F. Nazar, *Nat. Energy*, 2016, **1**, 16119.

8 C. K. Chan, H. L. Peng, R. D. Twesten, K. Jarausch, X. F. Zhang and Y. Cui, *Nano Lett.*, 2007, **7**, 490–495.

9 A. M. Cao, J. S. Hu, H. P. Liang and L. J. Wan, *Angew. Chem., Int. Ed.*, 2005, **44**, 4391–4395.

10 P. Senguttuvan, S.-D. Han, S. Kim, A. L. Lipson, S. Tepavcevic, T. T. Fister, I. D. Bloom, A. K. Burrell and C. S. Johnson, *Adv. Energy Mater.*, 2016, **6**, 1600826.

11 S. Park, C. W. Lee, J.-C. Kim, H. J. Song, H.-W. Shim, S. Lee and D.-W. Kim, *ACS Energy Lett.*, 2016, **1**, 216–224.

12 B. Yan, X. Li, Z. Bai, L. Lin, G. Chen, X. Song, D. Xiong, D. Li and X. Sun, *J. Mater. Chem. A*, 2017, **5**, 4850–4860.

13 Z. Khan, B. Senthilkumar, S. O. Park, S. Park, J. Yang, J. H. Lee, H.-K. Song, Y. Kim, S. K. Kwak and H. Ko, *J. Mater. Chem. A*, 2017, **5**, 2037–2044.

14 Z. Wu, W. Qiu, Y. Chen, Y. Luo, Y. Huang, Q. Lei, S. Guo, P. Liu, M.-S. Balogun and Y. Tong, *J. Mater. Chem. A*, 2017, **5**, 756–764.

15 G. Gershinsky, H. D. Yoo, Y. Gofer and D. Aurbach, *Langmuir*, 2013, **29**, 10964–10972.

16 L. D. Reed and E. Menke, *J. Electrochem. Soc.*, 2013, **160**, A915–A917.

17 H. Wang, Y. Bai, S. Chen, X. Luo, C. Wu, F. Wu, J. Lu and K. Amine, *ACS Appl. Mater. Interfaces*, 2014, **7**, 80–84.

18 S. Yang, Y. Gong, Z. Liu, L. Zhan, D. P. Hashim, L. Ma, R. Vajtai and P. M. Ajayan, *Nano Lett.*, 2013, **13**, 1596–1601.

19 C. Nethravathi, C. R. Rajamathi, M. Rajamathi, U. K. Gautam, X. Wang, D. Golberg and Y. Bando, *ACS Appl. Mater. Interfaces*, 2013, **5**, 2708–2714.

20 N. Bahlawane and D. Lenoble, *Chem. Vap. Deposition*, 2014, **20**, 299–311.

21 H. Li, P. He, Y. Wang, E. Hosono and H. Zhou, *J. Mater. Chem.*, 2011, **21**, 10999–11009.

22 Z. Y. Li and Q. H. Wu, *ChemPhysChem*, 2008, **9**, 300–304.

23 X. Rocquefelte, F. Boucher, P. Gressier and G. Ouvrard, *Chem. Mater.*, 2003, **15**, 1812–1819.

24 J. Braithwaite, C. Catlow, J. Gale and J. Harding, *Chem. Mater.*, 1999, **11**, 1990–1998.

25 Z. Wang, Q. Su and H. Deng, *Phys. Chem. Chem. Phys.*, 2013, **15**, 8705–8709.

26 X. Zhao, X. Zhang, D. Wu, H. Zhang, F. Ding and Z. Zhou, *J. Mater. Chem. A*, 2016, **4**, 16606–16611.

27 D. Wang, H. Liu, J. D. Elliott, L.-M. Liu and L. W. M. Lau, *J. Mater. Chem. A*, 2016, **4**, 12516–12525.

28 A. Parija, Y. Liang, J. L. Andrews, L. R. De Jesus, D. Prendergast and S. Banerjee, *Chem. Mater.*, 2016, **28**, 5611–5620.

29 V. Riffet, J. Contreras-García, J. Carrasco and M. Calatayud, *J. Phys. Chem. C*, 2016, **120**, 4259–4265.

30 J. Carrasco, *J. Phys. Chem. C*, 2014, **118**, 19599–19607.

31 V. V. Kulish, O. I. Malyi, C. Persson and P. Wu, *Phys. Chem. Chem. Phys.*, 2015, **17**, 13921–13928.

32 G. S. Gautam, P. Canepa, W. D. Richards, R. Malik and G. Ceder, *Nano Lett.*, 2016, **16**, 2426–2431.

33 G. S. Gautam, P. Canepa, A. Abdellahi, A. Urban, R. Malik and G. Ceder, *Chem. Mater.*, 2015, **27**, 3733–3742.

34 Z. Rong, R. Malik, P. Canepa, G. S. Gautam, M. Liu, A. Jain, K. Persson and G. Ceder, *Chem. Mater.*, 2015, **27**, 6016–6021.

35 G. S. Gautam, P. Canepa, R. Malik, M. Liu, K. Persson and G. Ceder, *Chem. Commun.*, 2015, **51**, 13619–13622.

36 B. Zhou, H. Shi, R. Cao, X. Zhang and Z. Jiang, *Phys. Chem. Chem. Phys.*, 2014, **16**, 18578–18585.

37 S. Lee, I. N. Ivanov, J. K. Keum and H. N. Lee, *Sci. Rep.*, 2016, **6**, 19621.

38 G. Kresse and J. Furthmüller, *Phys. Rev. B: Condens. Matter Mater. Phys.*, 1996, **54**, 11169–11186.

39 G. Kresse and D. Joubert, *Phys. Rev. B: Condens. Matter Mater. Phys.*, 1999, **59**, 1758–1775.

40 P. E. Blochl, *Phys. Rev. B: Condens. Matter Mater. Phys.*, 1994, **50**, 17953–17979.

41 J. P. Perdew, A. Ruzsinszky, G. I. Csonka, O. A. Vydrov, G. E. Scuseria, L. A. Constantin, X. Zhou and K. Burke, *Phys. Rev. Lett.*, 2008, **100**, 136406.

42 J. P. Perdew, K. Burke and M. Ernzerhof, *Phys. Rev. Lett.*, 1996, **77**, 3865–3868.

43 S. Grimme, *J. Comput. Chem.*, 2006, **27**, 1787–1799.

44 H. J. Monkhorst and J. D. Pack, *Phys. Rev. B: Solid State*, 1976, **13**, 5188–5192.

45 G. Henkelman, A. Arnaldsson and H. Jonsson, *Comput. Mater. Sci.*, 2006, **36**, 354–360.

46 G. Henkelman, B. P. Uberuaga and H. Jonsson, *J. Chem. Phys.*, 2000, **113**, 9901–9904.

47 S. L. Dudarev, G. A. Botton, S. Y. Savrasov, C. J. Humphreys and A. P. Sutton, *Phys. Rev. B: Condens. Matter Mater. Phys.*, 1998, **57**, 1505–1509.

48 L. Wang, T. Maxisch and G. Ceder, *Phys. Rev. B: Condens. Matter Mater. Phys.*, 2006, **73**, 195107.

49 D. Wang, L.-M. Liu, S.-J. Zhao, B.-H. Li, H. Liu and X.-F. Lang, *Phys. Chem. Chem. Phys.*, 2013, **15**, 9075–9083.

50 M. K. Aydinol, A. F. Kohan and G. Ceder, *J. Power Sources*, 1997, **68**, 664–668.

51 R. Enjalbert and J. Galy, *Acta Crystallogr., Sect. C: Cryst. Struct. Commun.*, 1986, **42**, 1467–1469.

52 C. Leroux, G. Nihoul and G. Van Tendeloo, *Phys. Rev. B: Condens. Matter Mater. Phys.*, 1998, **57**, 5111–5121.

53 W. Wang, B. Jiang, W. Xiong, H. Sun, Z. Lin, L. Hu, J. Tu, J. Hou, H. Zhu and S. Jiao, *Sci. Rep.*, 2013, **3**, 3383.

54 D. Panduwinata and J. D. Gale, *J. Mater. Chem.*, 2009, **19**, 3931–3940.

55 A. Moretti, F. Maroni, F. Nobili and S. Passerini, *J. Power Sources*, 2015, **293**, 1068–1072.

56 J. Shao, X. Li, Z. Wan, L. Zhang, Y. Ding, L. Zhang, Q. Qu and H. Zheng, *ACS Appl. Mater. Interfaces*, 2013, **5**, 7671–7675.

57 Q. An, Y. Li, H. D. Yoo, S. Chen, Q. Ru, L. Mai and Y. Yao, *Nano Energy*, 2015, **18**, 265–272.

58 W. H. Wan, Q. F. Zhang, Y. Cui and E. G. Wang, *J. Phys.: Condens. Matter*, 2010, **22**, 415501.